The Astrophysical Journal, 670:1391–1400, 2007 December 1

TWO JOVIAN-MASS PLANETS IN EARTHLIKE ORBITS[1]

Sarah E. Robinson,[2] Gregory Laughlin,[2] Steven S. Vogt,[2] Debra A. Fischer,[3] R. Paul Butler,[4]
Geoffrey W. Marcy,[5] Gregory W. Henry,[6] Peter Driscoll,[3,7]
Genya Takeda,[8] and John A. Johnson[5]
Received 2007 April 3; accepted 2007 July 29

ABSTRACT

We report the discovery of two new planets: a 1.94 $M_{\rm Jup}$ planet in a 1.8 yr orbit of HD 5319, and a 2.51 $M_{\rm Jup}$ planet in a 1.1 yr orbit of HD 75898. The measured eccentricities are 0.12 for HD 5319b and 0.10 for HD 75898b, and Markov chain Monte Carlo simulations based on the derived orbital parameters indicate that the radial velocities of both stars are consistent with circular planet orbits. With low eccentricity and 1 AU $< a <$ 2 AU, our new planets have orbits similar to terrestrial planets in the solar system. The radial velocity residuals of both stars have significant trends, likely arising from substellar or low-mass stellar companions.

Subject headings: planetary systems — stars: individual (HD 5319, HD 75898)

1. INTRODUCTION

Doppler searches for Jupiter-mass planets are nearly complete for semimajor axes 0.03 AU $\leq a \leq$ 3 AU. The distribution of exoplanet semimajor axes within this range reveals a paucity of planets orbiting less than 0.5 AU from their host stars (Butler et al. 2006). Instead, many giant planets are being found on terrestrial planet-like orbits, in or near the habitable zone: 25% of 212 known exoplanets within 100 pc have semimajor axes between 1.0 and 2.0 AU.[9] These observations suggest that planetary systems often have habitable zones dominated by gas giants. In this paper we announce the discovery of Jupiter-mass planets orbiting HD 5319 and HD 75898. Both planets have nearly circular orbits with semimajor axes between 1 and 2 AU.

HD 5319 and HD 75898 were selected for the Keck planet search after being flagged as metal-rich by the N2K consortium, on the basis of photometry and low-resolution spectroscopy (Ammons et al. 2006; Robinson et al. 2007). The N2K project's primary goal was to identify metal-rich stars likely to host hot Jupiters, which have high transit probabilities (Fischer et al. 2005). So far, one transiting hot Saturn (Sato et al. 2005) and six planets with periods $P < 15$ days (Wright et al. 2007; Johnson et al. 2006; Fischer et al. 2005, 2006) have been discovered among the N2K targets. However, the planet-metallicity correlation holds for all orbital periods, making the N2K target list a good source for discoveries of longer period planets as well. The new discoveries reported in this paper, HD 5319b and HD 75898b, are two of the seven intermediate-period planets so far found orbiting N2K target stars (see also Wright et al. 2007; Fischer et al. 2007).

In § 2 we report our observations and Keplerian fit to HD 5319. We discuss the HD 75898 system in § 3. In § 4 we discuss the implied presence of long-period stellar or substellar companions orbiting each star. We present a discussion and conclusions in § 5.

2. HD 5319

2.1. *Stellar Characteristics*

HD 5319 is a subgiant with $M_V = 3.05$, $V = 8.05$, $B - V = 0.985$, and a *Hipparcos* parallax (ESA 1997) of 0.010″, corresponding to a distance of 100 pc. High-resolution spectroscopic analysis (Valenti & Fischer 2005) yields $T_{\rm eff} = 5052 \pm 50$ K, $\log g = 3.57 \pm 0.15$, $v \sin i = 3.31 \pm 0.50$ km s^{-1}, and [Fe/H] $= 0.15 \pm 0.05$ dex. HD 5319's spectral type is listed as K0 III in the SIMBAD database and as G5 IV in the *Hipparcos* catalog. The star's M_V and $\log g$ values are most consistent with the G5 IV designation.

The luminosity is 4.6 $L_\odot$, including a bolometric correction of -0.259 (VandenBerg & Clem 2003). The luminosity and effective temperature imply a stellar radius of 2.8 $R_\odot$. We estimate stellar masses using theoretical stellar models based on the Yale Stellar Evolution Code as described in Takeda et al. (2007). The fine grid of evolutionary tracks has been tuned to the uniform spectroscopic analysis of Valenti & Fischer (2005) and provides posterior distributions for stellar mass, radius, gravity, and age. Based on this analysis, we derive a stellar mass of 1.56 $M_\odot$, a radius of 3.26 $R_\odot$, higher than implied by the bolometric luminosity, and an age of 2.4 Gyr for this subgiant. As a measure of uncertainty, the lower and upper 95% confidence intervals are provided in parentheses in Table 1 for the stellar mass, age, and radius.

Measurement of the core of the Ca H and K lines (Fig. 1) show that the star is chromospherically inactive. From 30 observations, we measure mean values of the Ca H and K indices of $S_{\rm HK} = 0.12$ and $\log R'_{\rm HK} = -5.34$. Based on the values of $S_{\rm HK}$ and $\log R'_{\rm HK}$, we derive a rotational period of $P_{\rm rot} = 19.0$ days (Noyes et al. 1984). However, we caution that the interpretation of $S_{\rm HK}$ and $\log R'_{\rm HK}$ and their correlation with $P_{\rm rot}$ may be subject to systematic errors for evolved stars, since the $P_{\rm rot}$ calibration was created for main-sequence stars.

[1] Based on observations obtained at the W. M. Keck Observatory, which is operated by the University of California and the California Institute of Technology. Keck time has been granted by NOAO and NASA.
[2] UCO/Lick Observatory, University of California at Santa Cruz, Santa Cruz, CA 95064; ser@ucolick.org.
[3] Department of Physics and Astronomy, San Francisco State University, San Francisco, CA 94132; fischer@stars.sfsu.edu.
[4] Department of Terrestrial Magnetism, Carnegie Institute of Washington DC, 5241 Broad Branch Road NW, Washington, DC 20015-1305.
[5] Department of Astronomy, University of California, Berkeley, CA 94720.
[6] Center of Excellence in Information Systems, Tennessee State University, 3500 John A. Merritt Boulevard, Box 9501, Nashville, TN 37209.
[7] Department of Earth and Planetary Sciences, Johns Hopkins University, Baltimore, MD 21218.
[8] Department of Physics and Astronomy, Northwestern University, 2145 Sheridan Road, Evanston, IL 60208.
[9] See catalog at http://exoplanets.org.

TABLE 1
Stellar Parameters

Parameter	HD 5319[a]	HD 75898[b]
V	8.05	8.03
M_V	3.05	3.49
$B - V$	0.985	0.626
Spectral type	G5 IV	G0 V
Distance (pc)	100.0	80.58
$L_\star$ ($L_\odot$)	4.6	3.0
[Fe/H]	0.15 (0.05)	0.27 (0.05)
$T_{\rm eff}$ (K)	5052 (50)	6021 (50)
$v \sin i$ (km s^{-1})	3.31 (0.50)	4.54 (0.50)
$\log g$	3.57 (0.15)	4.16 (0.15)
$M_\star$ ($M_\odot$)	(1.38) 1.56 (1.74)	(1.15) 1.28 (1.41)
$R_\star$ ($R_\odot$)	(2.85) 3.26 (3.76)	(1.42) 1.6 (1.78)
Age (Gyr)	(1.72) 2.40 (3.60)	(3.00) 3.80 (5.60)
$S_{\rm HK}$	0.12	0.15
$\log R'_{\rm HK}$	−5.34	−5.02
$P_{\rm rot}$ (days)	19.0	12.6
$\sigma_{\rm phot}$ (mag)	0.0017	0.0017

[a] Numbers in parentheses give 1 σ uncertainties of atmospheric parameter measurements.
[b] Double set of parentheses indicates 95% confidence intervals for stellar masses and radii.

We also monitored the star's brightness with the T12 0.8 m automatic photometric telescope (APT) at Fairborn Observatory (Henry 1999; Eaton et al. 2003). The T12 APT measures the brightness of program stars relative to nearby constant comparison stars with a typical precision of 0.0015–0.0020 mag for a single measurement. We obtained 89 Strömgren b and y brightness measurements spanning 438 days between 2004 October and 2006 January. The standard deviation of a single observation from the mean was 0.0017 mag, comparable to the measurement precision, which provides an upper limit to photometric variability in HD 5319. A periodogram analysis found no significant periodicity between 1 and 220 days. Thus, our photometry confirms the star's low level of chromospheric activity.

2.2. *Doppler Observations and Keplerian Fit*

Doppler observations were made at the Keck telescope using HIRES (Vogt et al. 1994) with an iodine cell to model the instrumental profile and to provide the wavelength scale (Butler et al. 1996). An exposure meter maintains a constant signal-to-noise ratio of about 200 in our spectra, yielding relatively uniform radial velocity (RV) precision. We obtained 30 observations of HD 5319. The observation dates, RVs, and measurement uncertainties are listed in Table 2 and plotted in Figure 2.

The periodogram of the RVs (Fig. 3) shows a strong, broad peak in the power spectrum, spanning 600–900 days. This peak is wide because of modest phase sampling for HD 5319b. To estimate the false alarm probability (FAP), the probability that the power in the highest peak is an artifact of noisy data or timing of observations, we use the bootstrap Monte Carlo method of Cumming (2004). We generated 10,000 data sets of noise using the measured stellar velocities, selected with replacements from residuals about the mean velocity, and calculated the periodogram for each synthetic RV data set. The fraction of trials with maximum periodogram power that exceeds the observed value gives the FAP (Cumming 2004). Figure 4 shows a histogram of the tallest peak height in each trial periodogram. Only 13 of 10,000 synthetic data sets yielded any peak with higher power than in the true periodogram, for FAP = 0.0013 (Table 3). The probability that the

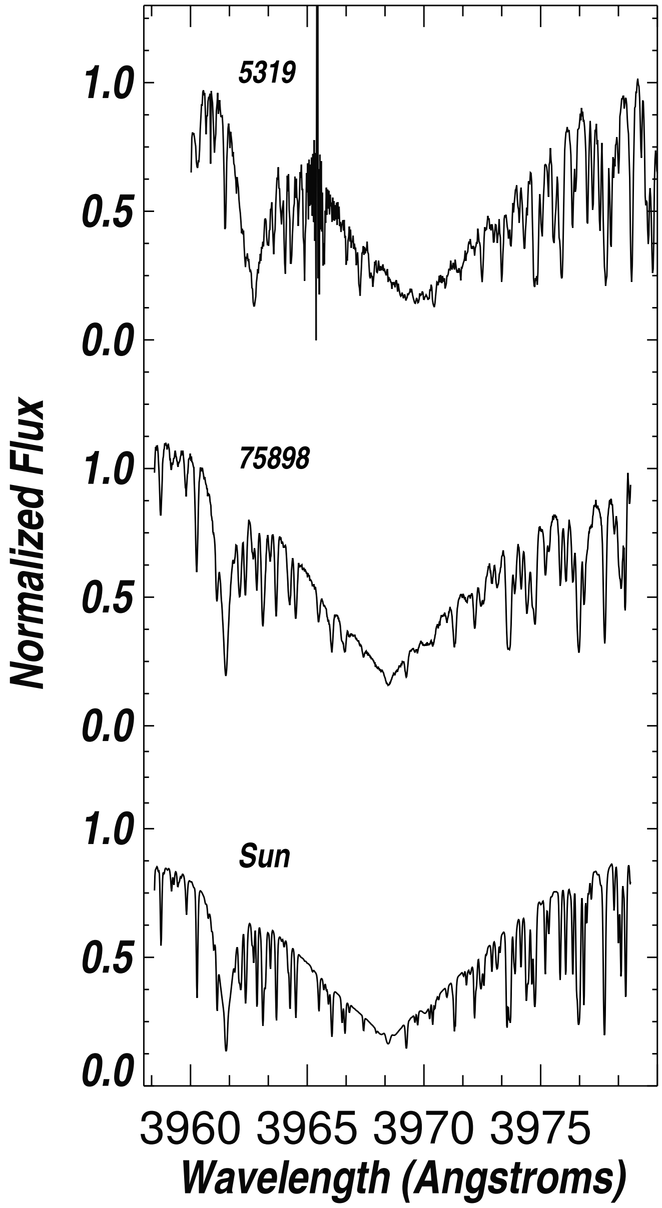

Fig. 1.—Ca II H line for HD 5319 and HD 75898, with the same wavelength segment of the solar spectrum shown for comparison. Both of these stars are chromospherically inactive, without emission in the cores of Ca II H and K.

600–900 day periodogram peak arises from a true physical source is therefore 99.87%, suggesting this period range should be searched for a Keplerian orbital fit.

The final task before determining the orbit of HD 5319b is to assess the astrophysical sources of error in RV measurements. In addition to velocity errors arising from our measurement uncertainties (including photon shot noise), the star itself can have cool spots, granular convective flows, or p-mode oscillations that contribute nondynamical velocity noise. These noise sources are collectively termed "jitter." For purposes of fitting a Keplerian model, the stellar jitter is added in quadrature to the formal instrumental errors. Jitter is not included in the tabulated measurement uncertainties for the RV sets.

We empirically estimate stellar jitter based on the chromospheric activity of the star and spectral type, following Wright (2005). The 20th percentile, median, and 80th percentile jitter amplitudes of stars at the chromospheric activity level and evolutionary stage of HD 5319 are 4.6, 5.7, and 9.5 m s^{-1}, respectively. We adopt the

TABLE 2
Radial Velocities for 5319

JD−2,440,000	RV (m s^{-1})	Uncertainty (m s^{-1})
13,014.75563	11.18	3.64
13,015.76065	20.26	3.43
13,016.76506	16.41	2.94
13,191.11010	−46.62	2.25
13,207.07543	−36.26	1.86
13,208.06565	−40.49	2.10
13,367.70779	−19.79	1.62
13,368.71602	−24.87	1.56
13,369.72525	−21.66	1.49
13,397.71935	−1.62	1.61
13,694.76591	20.56	1.60
13,695.77109	31.27	1.66
13,696.74616	31.53	1.68
13,724.77909	14.52	1.56
13,750.73625	18.19	1.57
13,775.72005	7.61	1.82
13,776.70605	3.29	1.81
13,777.72076	1.23	2.08
13,778.71684	−11.90	1.83
13,779.74125	5.89	1.93
13,927.04846	−19.25	1.70
13,933.04490	−23.28	1.87
13,959.09166	−16.17	2.05
13,961.03675	−13.30	1.77
13,961.04020	−13.63	1.88
13,981.90601	−20.45	1.87
14,023.77602	−10.05	1.92
14,083.83368	1.41	1.97
14,085.90265	10.07	1.99
14,129.77461	22.85	1.89

20th percentile value as a conservative jitter estimate (Table 1). The p-mode oscillation component of the jitter is $\sim$0.9 m s^{-1}, according to the solar scaling relation of Kjeldsen & Bedding (1995).

A Levenberg-Marquardt (LM) fitting algorithm was used to model the RVs of HD 5319. The best-fit Keplerian model gives an orbital period of 674.6 $\pm$ 16.9 days, with semivelocity amplitude $K = 33.6 \pm 4.3$ m s^{-1} and orbital eccentricity $e = 0.12 \pm 0.08$. We include a center of mass acceleration $dv/dt = 9.11$ m s^{-1} yr^{-1}, corresponding to a linear trend in the residual RVs. The best fit has rms $= 6.08$ m s^{-1} and $(\chi^2_\nu)^{1/2} = 1.22$, including 4.6 m s^{-1} for astrophysical jitter. Adopting a stellar mass of 1.56 $M_\odot$, we derive $M \sin i = 1.94$ $M_{\rm Jup}$ and semimajor axis $a = 1.75$ AU (angular separation $\alpha = 0.0175''$). The orbital solution is listed in Table 3, and the RV data are plotted with the best-fit Keplerian model (*solid line*) in Figure 2.

Uncertainties in the orbital parameters are first estimated with a model-based bootstrap Monte Carlo analysis. First, we find the best-fit Keplerian model. Then, for each of 250 trials, that theoretical best fit is subtracted from the observed RVs. The residual velocities are then scrambled (with replacement) and added back to the theoretical best-fit velocities and a new trial Keplerian fit is obtained. We adopt the standard deviation of each orbital parameter for the 250 Monte Carlo trials as the parameter uncertainty. The uncertainties of the Keplerian parameters of HD 5319b are listed in Table 3.

In order to confirm the orbital parameters of HD 5319b, a Markov chain Monte Carlo (MCMC) simulation was carried out for the HD 5319 velocities. This analysis, which gives posterior probability distribution for the orbital parameters, can be a useful

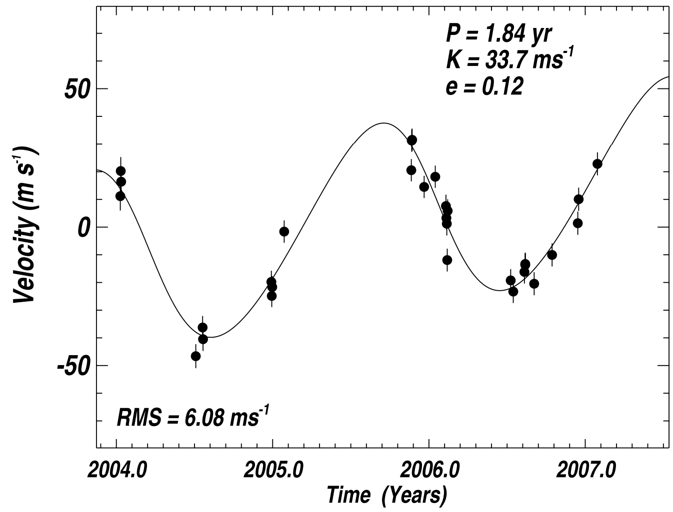

Fig. 2.—RVs for HD 5319. The velocity error bars show the single-measurement precision listed in Table 2, added in quadrature with 4.6 m s^{-1} stellar jitter. For a Keplerian fit plus a constant center-of-mass acceleration of 9.11 m s^{-1} yr^{-1}, $(\chi^2_\nu)^{1/2} = 1.22$. Assuming a stellar mass of 1.56 $M_\odot$, we derive a planet mass $M \sin i = 1.94$ $M_{\rm Jup}$, and a semimajor axis $a = 1.75$ AU.

check of the convergence of the LM fitting algorithm, particularly when the modeled $(\chi^2_\nu)^{1/2}$ space is confused with several local minima. For example, poor phase coverage might result in an aliased value of the period. A bimodal MCMC posterior distribution for the period would indicate the need for more observations to break the degeneracy.

Posterior probability distributions of P, e, and K are shown for HD 5319b in Figure 5. Because the orbit is nearly circular, the time of periastron passage and longitude of periastron are not well constrained, and the MCMC histograms are nearly flat. This ambiguity is also reflected in the large uncertainties ($\sim$1/8 orbit) for T_p and ω inferred from the orbit-based bootstrap simulations. The eccentricity distribution has mean $e = 0.09$, with our reported value of $e = 0.12$ lying within 1 σ of the mean. The mean of the period distribution, 686 days, is consistent with the period determined by the LM analysis, 675 days. The MCMC simulations settle on a somewhat larger value of velocity semiamplitude, $K = 39$ m s^{-1}, than the LM analysis ($K = 33.6$ m s^{-1}), a difference of 1.4 σ.

To assess the wisdom of adding the extra term dv/dt to our fit, we perform a statistical test for an additional term (Bevington & Robinson 1992). We define $\Delta\chi^2$ as the difference in unreduced

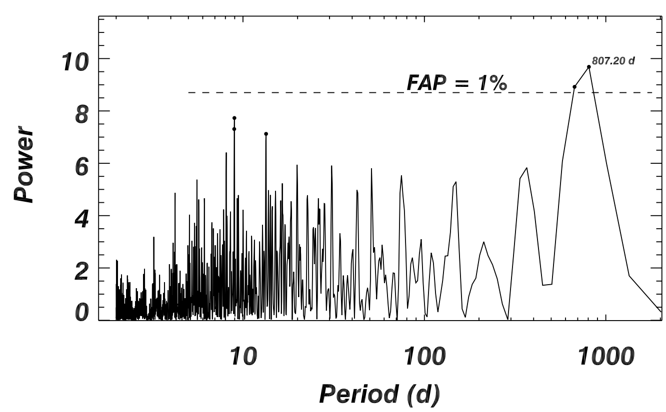

Fig. 3.—Periodogram of HD 5319 RVs. The strong peak spanning 600–900 days has FAP = 0.0013, giving a 99.87% probability that this peak has a physical, non-noise source.

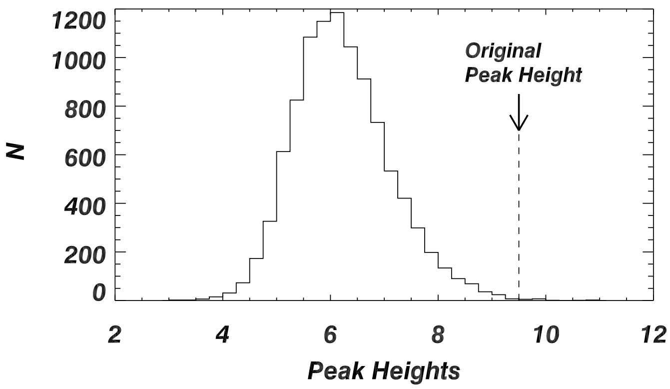

FIG. 4.—FAP determination for HD 5319. Histogram shows maximum periodogram peak heights in 10,000 synthetic RV data sets, selected with replacement from the measured RVs. Only 13 trials yielded a maximum power greater than the original periodogram, for FAP = 0.0013.

χ^2 between the best fits obtained with and without the dv/dt term, and χ^2_ν as the reduced χ^2 of the published fit, including dv/dt. The quantity

$$F = \frac{\Delta\chi^2}{\chi^2_\nu} \quad (1)$$

follows an F-distribution with one numerator degree of freedom and $\nu = N_{\rm obs} - 7$ denominator degrees of freedom, where $N_{\rm obs}$ is the number of observations (30 for HD 5319). The best fit obtained without the dv/dt term has $\chi^2 = 61.4$ $[(\chi^2_\nu)^{1/2} = 1.60]$, giving $F = 18.2$. The probability $P(F; 1, 23)$ that a randomly selected F exceeds this value is 0.00029, for a less than 1 in 1000 chance that the fit improvement provided by the dv/dt term is spurious. Therefore, there is strong evidence that a long-period companion is accelerating the center of mass of the HD 5319a-b system.

Noticing a smooth variation in the residuals of a one-planet fit, one might be tempted to fit a second Keplerian with a longer period. However, in the case of HD 5319, this is premature: the linear correlation coefficient of the one-planet residuals is 0.85, indicating that a linear model describes the variation in these residuals well. We do not yet detect any curvature in the RV signature of the second companion, so we refrain from fitting a full Keplerian or a circular orbit. We allow the period of this long-period companion to remain undetermined, and approximate its effects on the system with a constant acceleration dv/dt.

3. HD 75898

3.1. *Stellar Characteristics*

HD 75898 has $V = 8.03$, $B - V = 0.626$, and a *Hipparcos* parallax (ESA 1997) of $0.012''$, corresponding to a distance of 80.6 pc. Spectroscopic analysis yields $T_{\rm eff} = 6021 \pm 50$ K, $\log g = 4.16 \pm 0.15$, $v \sin i = 4.54 \pm 0.50$ km s^{-1}, and $[{\rm Fe/H}] = 0.27 \pm 0.05$ dex. The absolute visual magnitude is $M_V = 3.49$, and the luminosity is 3.0 $L_\odot$ (with a bolometric correction of -0.039). Although the SIMBAD spectral type designation is G0 V, the luminosity, temperature and surface gravity are more consistent with a metal-rich F8 V star. The value of M_V indicates that the star is just beginning to evolve onto the subgiant branch. From the stellar luminosity and surface gravity, we derive a stellar radius of 1.6 $R_\odot$, identical to the radius derived from evolutionary tracks. A stellar mass of 1.28 $M_\odot$ and an age of 3.8 Gyr are derived from evolutionary tracks (Takeda et al. 2007). The physical parameters of HD 75898 are listed in Table 1.

TABLE 3
ORBITAL PARAMETERS

Parameter	HD 5319	HD 75898
P (days)	674.6 (17)[a]	418.2 (5.7)
T_p (JD−2,440,000)	13,067.7 (77)	12,907.0 (37)
ω (deg)	76.3 (35)	263.7 (30)
Ecc	0.12 (0.08)	0.10 (0.05)
K_1 (m s^{-1})	33.6 (4.3)	58.2 (3.1)
dv/dt (m s^{-1} days^{-1})	0.0249 (0.0040)	−0.0400 (0.0056)
a (AU)	1.75	1.19
$a_1 \sin i$ (AU)	0.00207	0.00222
$f_1(m)$ ($M_\odot$)	2.37E−09	8.39E−09
$M \sin i$ ($M_{\rm Jup}$)	1.94	2.51
$N_{\rm obs}$	30	20
Assumed jitter (m s^{-1})	4.6	2.6
rms (m s^{-1})	6.08	5.48
Reduced $(\chi^2_\nu)^{1/2}$	1.22	1.77
FAP	0.0013	<0.0001

[a] Uncertainties of Keplerian orbital parameters are given in parentheses.

HD 75898 was selected for the Keck planet search after being observed by the N2K low-resolution spectroscopic survey (Robinson et al. 2007), carried out at the 2.1 m telescope at KPNO from 2004 August to 2005 April. The atmospheric parameters measured from N2K spectra were $T_{\rm eff} = 5983 \pm 82$ K, $[{\rm Fe/H}] = 0.22 \pm 0.07$ dex, and $\log g = 4.22 \pm 0.13$ dex. These values agree with the Keck measurements within uncertainties.

Figure 1 shows that the star is chromospherically inactive, with no observed emission in Ca II H and K. We derive mean $S_{\rm HK} = 0.15$ and $\log R'_{\rm HK} = -5.02$, with a corresponding rotational period $P_{\rm rot} = 12.6$ days. The caution that the $P_{\rm rot}$ measurement may be affected by systematic errors for evolved stars applies to HD 75898 as well, since this star is beginning to move off the main sequence. Wright (2005) reports 20th percentile, median, and 80th percentile jitter amplitudes of 2.6, 4.0, and 6.2 m s^{-1}, for stars with similar activity level and evolutionary stage to HD 75898. Again, we adopt a conservative, 20th percentile jitter estimate of 2.6 m s^{-1} (Table 1). The p-mode oscillation component of the jitter is ~0.5 m s^{-1} (Kjeldsen & Bedding 1995). The stellar characteristics are summarized in Table 1.

We monitored the brightness of HD 75898 with the T12 0.8 m APT (Henry 1999; Eaton et. al 2003). We obtained 26 good b and y photometric measurements spanning 85 days between 2007 March and May. The standard deviation of a single observation from the mean was 0.0017 mag, comparable to our measurement precision, which provides an upper limit to photometric variability in HD 75898. A periodogram analysis found no significant periodicity between 1 and 40 days; in particular, no variability was detected around the estimated rotation period of 12.6 days. Thus, our photometry confirms the star's low level of chromospheric activity.

3.2. *Doppler Observations and Keplerian Fit*

We obtained 20 observations of HD 75898. Observation dates, RVs, and instrumental uncertainties in the RVs (not including stellar jitter) are listed in Table 4. The periodogram for this data set (Fig. 6) shows a strong peak at 446 days. Once again, we calculate the FAP by sampling the observed RVs with replacement, keeping the original observation times, and calculating the maximum periodogam power for the scrambled velocities. In 10,000 synthetic data sets, no periodogram had higher power than the original 446 day peak. The FAP for this peak is <0.0001 (Table 3), indicating a better than 0.9999 probability that the periodicity in

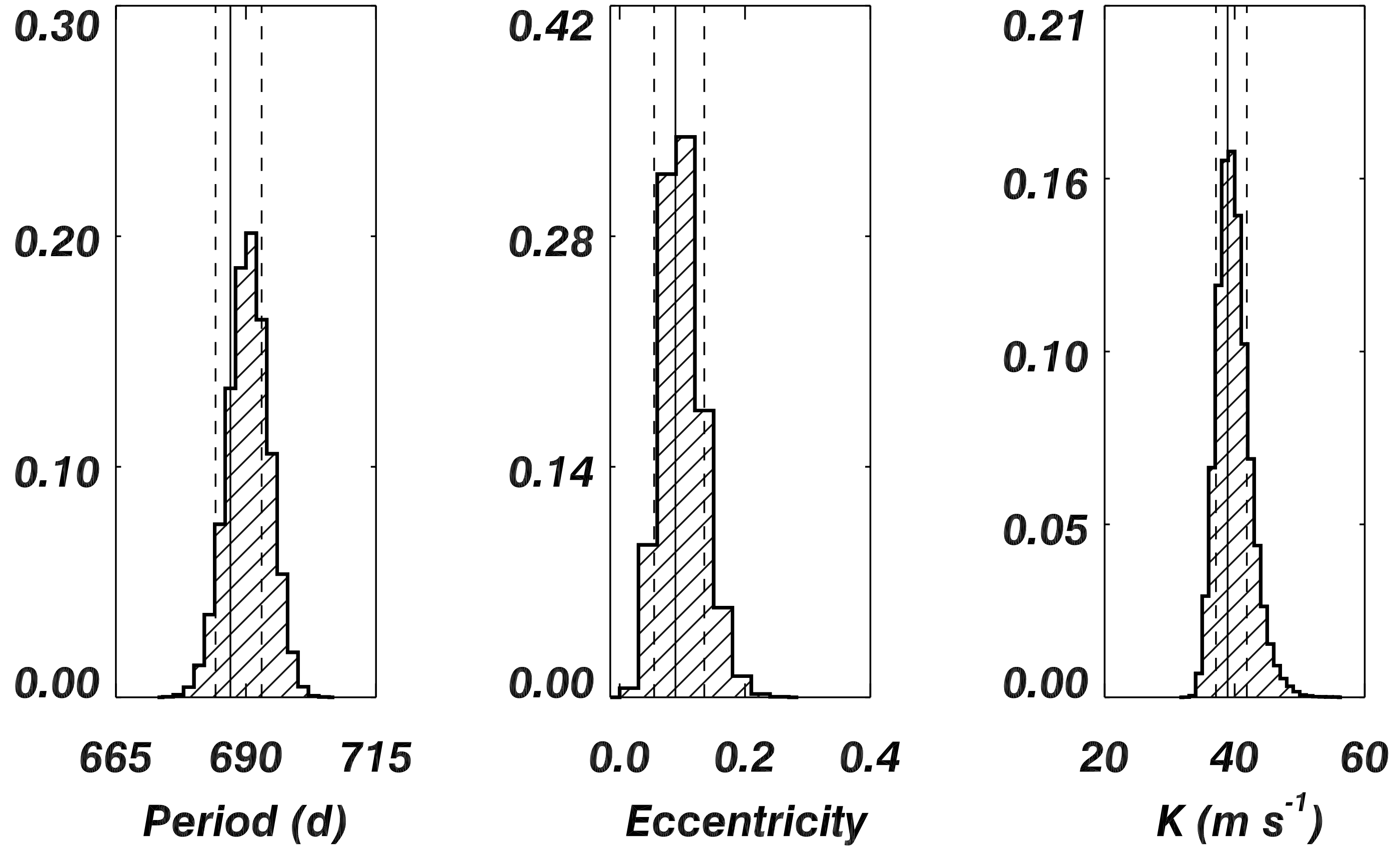

FIG. 5.—MCMC models of the RV data for HD 5319 produce posterior distributions for the orbital period, eccentricity, and RV semiamplitude. The mean values of each MCMC histogram are broadly consistent with the Keplerian parameters determined by the LM algorithm, and show convergence to a single set of orbital parameters.

RVs has an astrophysical source, and is not caused by noise. The histogram of periodogram power in the tallest periodogram peak in each of 10,000 trials is plotted in Figure 7.

There is also a peak in the periodogram at 200 days, which may be an alias of the true, ~400 day period; an artifact of the $\frac{1}{2}$ yr observing season of HD 75898, which is near the ecliptic. Two other possible explanations for the 200 day peak are that it arises from the modest eccentricity ($e \approx 0.1$) of the best-fit 418 day orbit, or that there is a second planet in the system with a period near 200 days. The observations between 2004 January and 2006 May, which do not include the minimum of the RV curve, can be modeled credibly with Keplerian orbits of either ~200 or ~400 days. However, when the four most recent observations, which do

TABLE 4
Radial Velocities for 75898

JD−2,440,000	RV (m s^{-1})	Uncertainty (m s^{-1})
13,014.94581	74.84	2.11
13,015.94526	70.75	1.95
13,016.95038	75.31	2.22
13,071.85048	49.86	2.47
13,398.05874	48.47	1.48
13,480.81249	33.98	1.85
13,724.06020	−41.40	1.47
13,747.02281	−15.98	1.70
13,747.95543	−12.07	1.75
13,748.91982	−3.75	1.73
13,749.85611	−12.29	1.31
13,750.86351	−22.30	1.64
13,752.96966	−11.73	1.27
13,775.92652	15.00	1.48
13,776.94321	8.26	1.88
13,841.81102	44.55	1.91
14,083.98611	−84.77	1.39
14,084.91551	−80.23	1.47
14,086.10668	−89.70	1.45
14,129.98648	−69.14	1.52

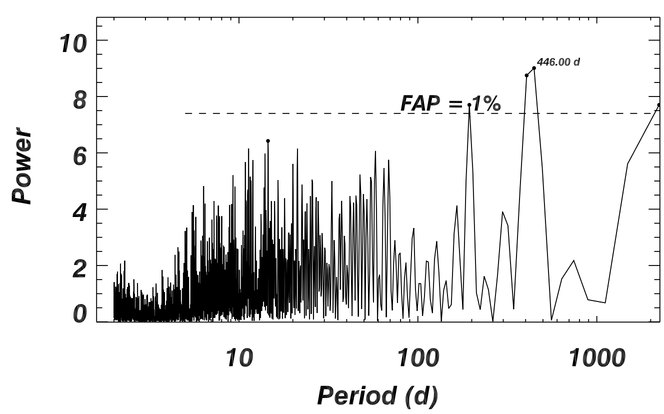

FIG. 6.—Periodogram of HD 75898 RVs. The peak at 446 days has FAP < 0.0001. The 200 day peak is an alias of the true, ~400 day period; the artifact of the 7 month observing season for this star is near the ecliptic. The observations in late 2006 and early 2007 break this alias and rule out a 200 day period for HD 75898b. The rising power toward 2000 days, twice our observational baseline, is the first hint of a third component of the HD 75898 system (see § 4 for details).

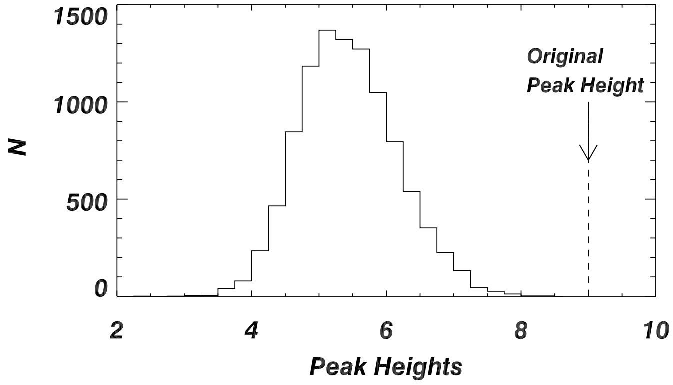

FIG. 7.—FAP determination for HD 75898. Histogram shows maximum periodogram peak heights in 10,000 synthetic data sets, selected with replacement from the measured RVs. No trial yielded a maximum power greater than the original periodogram, for FAP < 0.0001.

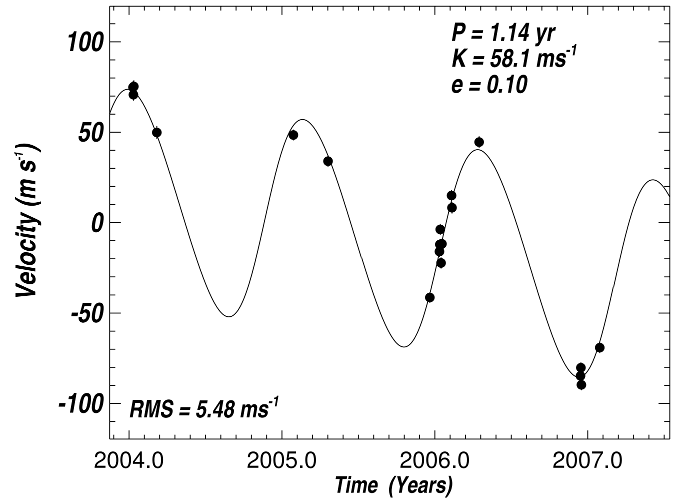

FIG. 8.—RVs for HD 75898. The velocity error bars show the single measurement precision given in Table 2, added in quadrature with 2.6 m s^{-1} stellar jitter. This gives $(\chi_\nu^2)^{1/2} = 1.77$ for the Keplerian fit, with a residual linear trend of -14.6 m s^{-1} yr^{-1}. Assuming a stellar mass of 1.28 $M_\odot$, we derive a planet mass $M \sin i = 2.51$ $M_{\rm Jup}$, and semimajor axis $a = 1.19$ AU.

cover the RV minimum, are included, the degeneracy is broken and single planets with 200 day orbits do not fit the data.

The best-fit Keplerian model gives a period of 418.2 ± 5.7 days, with semivelocity amplitude $K = 58.2 \pm 3.1$ m s^{-1}, and orbital eccentricity $e = 0.10 \pm 0.05$. The rms to the fit is 5.48 m s^{-1} with $(\chi_\nu^2)^{1/2} = 1.77$, including the estimated astrophysical jitter of 2.6 m s^{-1}. Adopting a stellar mass of 1.28 $M_\odot$, we derive $M \sin i =$ 2.51 $M_{\rm Jup}$. The corresponding semimajor axis is $a = 1.19$ AU, and the angular separation is $\alpha = 0.0148''$. The residual velocities show a strong trend, $dv/dt = -14.6$ m s^{-1} yr^{-1}, suggesting that an additional companion orbits the star. The Keplerian orbital parameters are listed in Table 3 and plotted with the best-fit Keplerian model (*solid line*) in Figure 8.

To assess whether the constant acceleration dv/dt should be included in the fit, we again perform the test for an additional term given in equation (1). The best-fit Keplerian without the dv/dt term has $\chi^2 = 142.5$ ($(\chi_\nu^2)^{1/2} = 3.19$). The F-statistic comparing the best fits with and without dv/dt is 32.5. There are 20 observations of this star, giving the F distribution 13 denominator degrees of freedom. The probability $P(F; 1, 13)$ that the fit improvement from including dv/dt is spurious is only 7.3×10^{-5}. The detected acceleration of the HD 75898a-b center of mass is therefore almost certainly real, and not an artifact of noise. Further evidence for a long-period companion to HD 75898 is provided by the periodogram, which rises toward a 2000 day period (almost twice the length of our observational baseline). The correlation coefficient for a linear fit to the single-planet residuals is $r = -0.96$, indicating that variation in RV residuals is well described by a constant acceleration. The relatively sparse sampling precludes detection of curvature from any additional planets at this time.

We carried out a MCMC simulation for the RV residuals of HD 75898. The resulting posterior distributions for period, RV semiamplitude, and eccentricity are shown in Figure 9. For this low-eccentricity orbit, time of periastron passage and longitude of periastron are not well constrained. The fact that the MCMC eccentricity distribution peaks at zero suggests that the orbit of HD 75898b could in fact be circular. The mean eccentricity in the MCMC posterior distribution is 0.1, in agreement with the LM value of 0.10 ± 0.05. The mean of the MCMC period distribution is 417 days, which is well matched with the results of the LM analysis ($P = 418$ days). For velocity semiamplitude K, the MCMC results also reproduce the LM results, with mean $K = 58$ m s^{-1}.

Being near the ecliptic ($\delta = 33°$), with a period near 1 yr (418 days), HD 75898 presents a special hazard for planet detection. The observing season for HD 75898 is just 7 months, so only half of the orbital phase is visible during 1 yr. At the same time, the visible phase of HD 75898b's orbit advances only 12% per year. Although our observational baseline covers 3 yr and two-thirds of the orbit, it would take 5 yr to obtain full phase coverage. We expect the orbital solution to be revised as more observations of HD 75898 are obtained.

Observations near periastron passage contain the most information about the orbit, particularly eccentricity (e.g., Endl et al. 2006). If our best-fit orbit is correct, we have observed the periastron passage to within 4 days (JD 2453747). This fact, combined with the results of the MCMC simulation for eccentricity, leads us to believe that our basic discovery is correct, that HD 75898 has a planet with a minimum mass of 2 $M_{\rm Jup}$ in a nearly circular orbit near 1 AU.

4. LONG-PERIOD COMPANIONS

The RV residuals of HD 5319 and HD 75898 have significant linear trends, $|dv/dt| \geq 9$ m s^{-1} yr^{-1}. This indicates that the center of mass of each two-body system is accelerating, which cannot happen unless there is a third component in each system. Both stars, then, show evidence of long-period companions with incomplete phase coverage during our observational baseline. The possibility of finding brown dwarfs orbiting Sun-like stars is a tantalizing one, warranting further analysis of the one-planet residuals of HD 5319 and HD 75898. Brown dwarf companions might reside in the brown dwarf desert (McCarthy & Zuckerman 2004; Grether & Lineweaver 2006), the dearth of substellar companions to main-sequence stars with $a < 1200$ AU. Another possibility is that the third components are giant planets with $P \gtrsim 2000$ days. Even the presence of stellar companions would make HD 5319 and HD 75898 unusual planet hosts, as new evidence indicates planet occurrence is infrequent in binaries closer than 120 AU (Eggenberger & Udry 2007). In this section, we analyze possible configurations of the HD 5319 and HD 75898 systems.

The possible companion types—planets, brown dwarfs, and stars—are restricted to a particular semimajor axis range by the measured dv/dt and the long-term dynamical stability of each system. Although these ranges overlap substantially when all potential variations in time of periastron passage, line of apsides, and

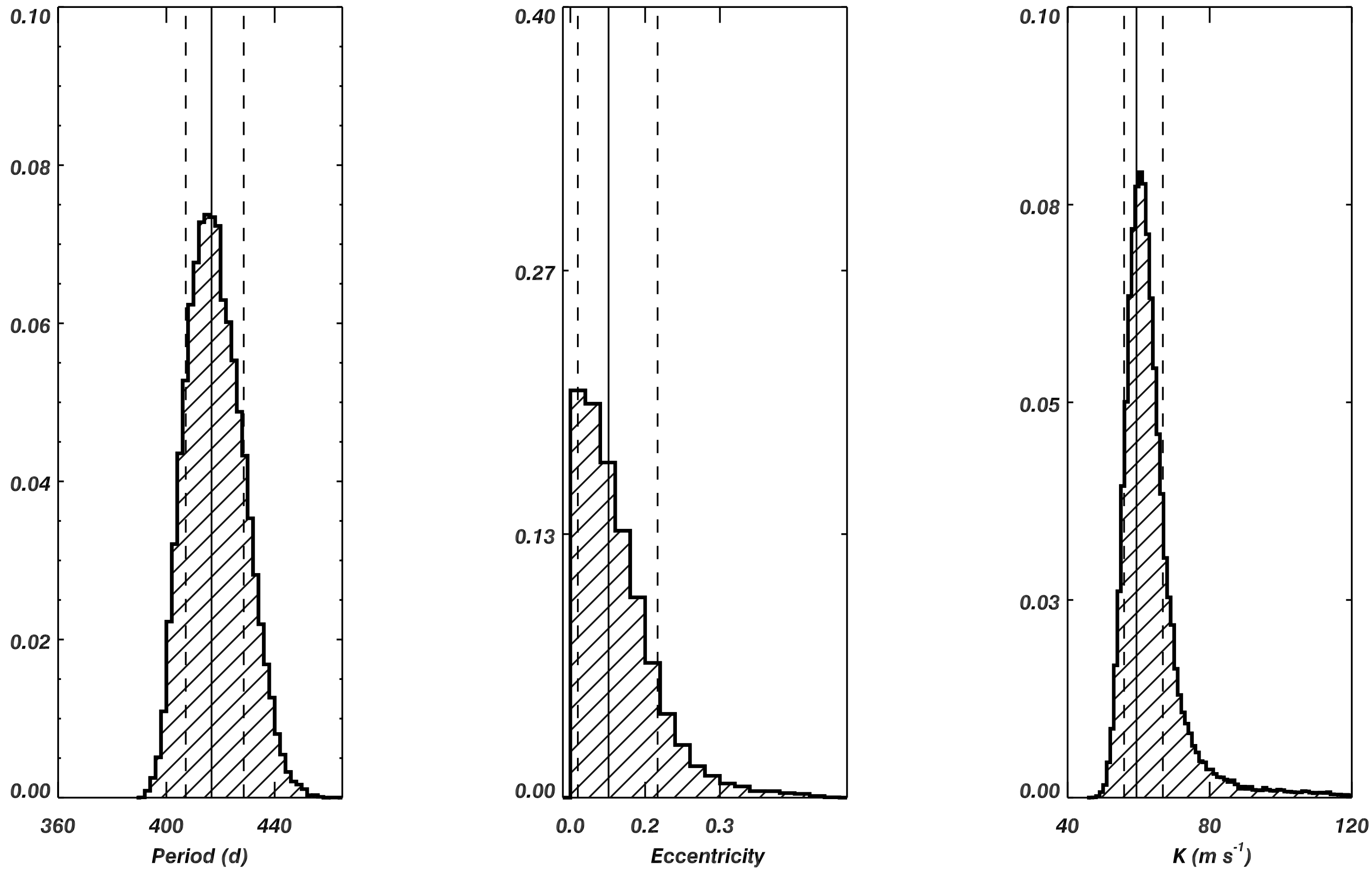

FIG. 9.—MCMC posterior distributions for the period, eccentricity, and RV semiamplitude of HD 75898. The mean of each distribution is well matched with the corresponding result from our LM analysis.

eccentricity are taken into account, the general pattern is $a_* \gtrsim a_{\rm bd} \gtrsim a_{\rm planet}$. This pattern can be illustrated by the simple example of a circular orbit: the star reaches RV semiamplitude when the planet has moved one-quarter orbit from its ephemeris, so we can calculate the approximate semiamplitude by

$$K \approx \left(\frac{P}{4}\right)\frac{dv}{dt}. \qquad (2)$$

Equation (2) shows that the longer a star maintains the measured constant dv/dt, the higher the mass of the companion. For eccentric orbits, the proportionality constant relating K and P changes, but the pattern $a_* \gtrsim a_{\rm bd} \gtrsim a_{\rm planet}$ holds.

The smallest possible semimajor axis for component c, $a_{\rm min}$, is determined by the requirement that the two companions in each system do not experience close encounters, which could lead to large perturbations of both orbits. Absent any dynamical considerations, $a_{\rm min}$ would correspond to a highly eccentric orbit with the apoastron passage near the midpoint of our observations, and with a period only slightly longer than our time baseline. However, the more eccentric the outer component's orbit, the nearer its approach to the inner planet during periastron passage.

Assuming nonresonant systems, we can set a lower limit to the distance of closest approach between components b and c. David et al. (2003) examine of the stability of a two-planet system, with an intermediate-mass companion exterior to an Earth-mass planet on a circular orbit at 1 AU. They find that an outer planet with mass 1 $M_{\rm Jup}$ and $R_{\rm peri} \sim 2.5$ AU give a mean ejection time of 1 Gyr for the terrestrial planet. Although HD 5319 and HD 75898 have far more massive inner planets than the theoretical system of David et al., we apply their analysis because of the similar orbits of the inner planets in all three systems. Adopting the 1 Gyr stability criterion, we set the minimum periastron distance of the c component as $R_{\rm min} \geq 2.5a_{\rm inner}$. For each component type (planet, brown dwarf, and star), the orbit corresponding to $a_{\rm min}$ must obey this stability criterion and reproduce the observed dv/dt within uncertainties.

In this section, we refer to HD 5319c, HD 75898c as "the c components." We use this nomenclature as shorthand for "implied long-period companion," and are not claiming actual detections of these objects.

4.1. *Planet Orbits*

If HD 5319c or HD 75898c is a planet, $a_{\rm min}$ is simply the stability limit $R = 2.5a_{\rm inner}$, and the orbit associated with $a_{\rm min}$ is circular. We note that giant planets on circular orbits can have semimajor axis ratios less than 2.5, as Jupiter and Saturn do, but $a_{\rm outer}/a_{\rm inner} < 2$ is rare among exoplanets (Butler et al. 2006). To find the minimum planet mass for HD 5319c and HD 75898c, we substitute test values of $M \sin i$ into the equations

$$\left(\frac{a}{\rm AU}\right)^3 = \left(\frac{M_\star + M \sin i}{M_\odot}\right)\left(\frac{P}{\rm yr}\right)^2, \qquad (3)$$

$$M \sin i = K\sqrt{1-e^2}\left[\frac{P(M_\star + M \sin i)^2}{2\pi G}\right]^{1/3}, \qquad (4)$$

and use the resulting value of K to calculate a RV curve. Here $M_{\rm min,\, planet}$ is the lowest value of $M \sin i$ for which the RV slope,

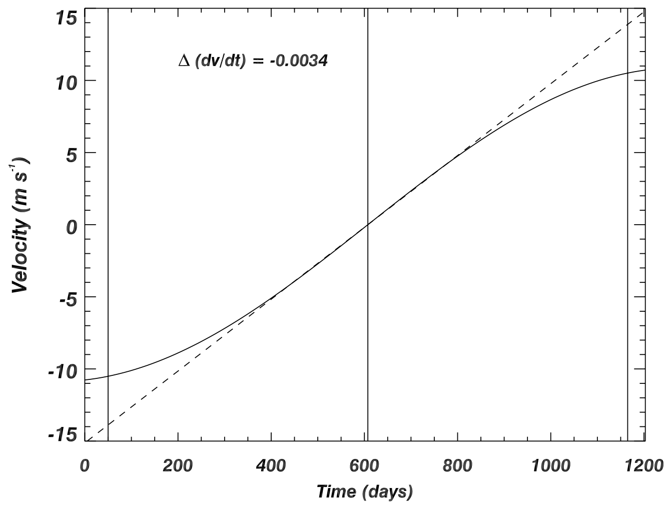

FIG. 10.—Theoretical RV curve of HD 5319c at its smallest possible mass and period, $M \sin i = 1.0\ M_{\rm Jup}$ and $P = 7.3$ yr. Vertical lines denote the beginning, midpoint, and end of our observational baseline. The dashed line shows the center-of-mass acceleration, 0.0249 m s^{-1} day^{-1}. The difference between the linear slope of this theoretical RV curve and the measured dv/dt, $|\Delta(dv/dt)| = 0.0034$, is less than the uncertainty in dv/dt (0.0040 m s^{-1} day^{-1}).

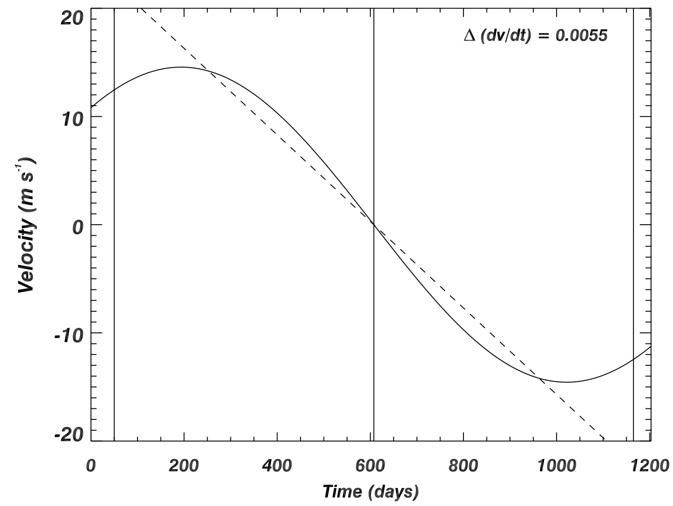

FIG. 11.—Theoretical RV curve of HD 75898c at its shortest possible period, 4.5 yr, and smallest mass, 1 $M_{\rm Jup}$. Vertical lines denote the beginning, midpoint and end of our observational baseline. The dashed line shows the center-of-mass acceleration, -0.0400 m s^{-1} day^{-1}. The difference between the linear slope of this theoretical RV curve and the measured dv/dt, $|\Delta(dv/dt)| = 0.0055$, is consistent with the measured uncertainty $\sigma(dv/dt) = 0.0056$ m s^{-1} day^{1}.

determined from a linear fit, matches the observed dv/dt within the uncertainties reported in Table 3: $|dv/dt_{\rm calc} - dv/dt_{\rm obs}| \leq \sigma(dv/dt)$.

The minimum mass of HD 5319c is 1.0 $M_{\rm Jup}$. This planet would reside at $a = 4.4$ AU, and have a period of 2675 days (7.3 yr). Figure 10 shows the RV curve corresponding to this orbit, together with the observed trend in the fit residuals of HD 5319b. HD 75898c also has a minimum mass $M_{\rm min} = 1.0\ M_{\rm Jup}$, in a circular orbit with semimajor axis $a = 3.0$ AU and $P = 1656$ days (4.5 yr). The resulting RV curve, plus the measured trend in the HD 75898b residuals, are shown in Figure 11. These orbital solutions show that HD 5319c and HD 75898c could be similar, in mass, semimajor axis, and perhaps equilibrium temperature, to Jupiter.

For the maximum possible planet mass of HD 5319c or HD 75898c, we adopt the IAU criterion that a planet does not burn deuterium, and so $M_{\rm max} = 13\ M_{\rm Jup}$ (Boss et al. 2007). We can calculate $a_{\rm max}$ and $P_{\rm max}$ for this borderline planet by examining the limiting case where the periastron passage, which coincides with ephemeris, occurs at the midpoint of our observations. This is the part of the RV curve that varies most rapidly. In principle, $a_{\rm max}$ and $P_{\rm max}$ could become arbitrarily large as $e \rightarrow 1$. We adopt the convention of Patel et al. (2007) and define $e_{\rm max} = 0.8$, since 90% of spectrosopic binaries with $P > 10$ yr have $e < 0.8$ (Pourbaix et al. 2004).

To calculate $a_{\rm max}$ for planet orbits, we substitute test values of a into equations (3) and (4), and use the resulting value of K to calculate a RV curve. We then find the maximum a for which $|dv/dt_{\rm calc} - dv/dt_{\rm obs}| \leq \sigma(dv/dt)$. For HD 5319c, $a_{\rm max} = 85$ AU, corresponding to a period of 625 yr. For HD 75898c, $a_{\rm max} = 65$ AU and $P_{\rm max} = 460$ yr. In practice, it is extremely unlikely that either object is a planet on this type of orbit: the probability of catching these long-period, eccentric orbits exactly at periastron passage is quite low. The ranges of possible planet orbits for HD 5319c and HD 75898c are summarized in Table 5.

4.2. *Brown Dwarf Orbits*

To find $a_{\rm min}$ for brown dwarf orbits, we examine the limiting case where apoastron coincides with ephemeris at the midpoint of our observational baseline. This configuration gives the RV curve that most nearly approximates a straight line. Recalling that high mass implies high semimajor axis (cf. eq. [2]), we set $M \sin i = 13\ M_{\rm Jup}$, the minimum possible brown dwarf mass. Substituting test values of a and e into equations (3) and (4), we find the semiamplitude K for each a, e pair that meets the stability criterion $a(1 - e) \geq 2.5 a_{\rm inner}$. The linear slopes of the resulting RV curves are examined to find the minimum a where $\Delta(dv/dt) \leq \sigma(dv/dt)$ (Table 3). For HD 5319c, $a_{\rm min} = 9.8$ AU for a brown dwarf. This orbit has $e = 0.55$ and $P = 24$ yr. If HD 75898c is a brown dwarf, $a_{\rm min} = 7.5$ AU and $P_{\rm min} = 18$ yr, with eccentricity $e = 0.60$.

We determine $a_{\rm max}$ for brown dwarf orbits by setting $M \sin i = 83.8\ M_{\rm Jup}$, the minimum mass for hydrogen fusion. We follow the same method outlined in § 4.1 for finding $a_{\rm max}$, once again assuming $e_{\rm max} = 0.8$. For HD 5319c, $a_{\rm max} = 190$ AU and $P_{\rm max} = 2045$ yr for brown dwarf orbits. For HD 75898c, $a_{\rm max} = 170$ AU and $P_{\rm max} = 1900$ yr.

We note that the brown dwarf semimajor axis ranges implied by our measured dv/dt, 9.8 AU $\lesssim a \lesssim$ 190 AU for HD 5319c and 7.5 AU $\lesssim a \lesssim$ 170 AU for HD 5319c, fall directly in the brown dwarf desert (McCarthy & Zuckerman 2004). The ranges of possible brown dwarf periods and semimajor axes for HD 5319c and HD 75898c are summarized in Table 5.

4.3. *Star Orbits*

To find $a_{\rm min}$ for stellar companions to HD 5319 and HD 75898, we set $M \sin i = 83.8\ M_{\rm Jup}$, the minimum mass for a main-sequence star. Once again, we set the apoastron passage to coincide with the ephemeris and place it at the midpoint of our observations, finding the best approximation to a linear RV curve. We follow the procedure outlined in § 4.2, testing a grid of a and e values which meet the stability criterion and finding the minimum a for which the linear RV slope matches our measured dv/dt within uncertainties (Table 3). The minimum semimajor axis for HD 5319c, if it is a star, is $a_{\rm min} = 22$ AU, with $P_{\rm min} = 81$ yr and $e = 0.8$. For HD 75898c, $a_{{\rm min},\star} = 17$ AU, $P_{{\rm min},\star} = 58$ yr, and $e = 0.8$.

TABLE 5
Constraints on Orbits of Implied Long-Period Components

Parameter Range	HD 5319c[a]	HD 75898c[b]
Star		
$M \sin i$ ($M_\odot$)	0.08–0.65	0.08–0.60
a (AU)	22–630	17–470
P (yr)	81–10600	58–7400
Brown Dwarf		
$M \sin i$ ($M_{\rm Jup}$)	13–83.8	13–83.8
a (AU)	9.8–190	75–170
P (yr)	24–2045	18–1900
Planet		
$M \sin i$ ($M_{\rm Jup}$)	1.0–13	1.0–13
a (AU)	4.4–85	3.0–65
P (yr)	7.3–625	4.5–460

[a] Each entry in this table gives the minimum and maximum values a particular parameter can assume, according to the measured center-of-mass acceleration and stability constraints.
[b] Maximum periods and semimajor axes for each object class are calculated assuming $e_{\rm max} = 0.8$ (see § 4.1 for discussion).

We determine the maximum masses of stellar companions to HD 5319 and HD 75898 by noting that neither star was identified as a double-lined spectroscopic binary (SB2) in the Keck spectra. The minimum flux ratio for detecting SB2s with HIRES is $\sim$0.01. This limit gives $M_V > 8.05$ HD 5319c and $M_V > 8.49$ HD 75898c. The corresponding masses are $M \sin i = 0.65\ M_\odot$ and $M \sin i = 0.6\ M_\odot$, respectively (Yi et al. 2001). Assuming that the periastron passage and ephemeris fall at the midpoint of our observations and $e_{\rm max} = 0.8$, HD 5319c has $a_{\rm max} = 630$ AU and $P_{\rm max} = 10{,}600$ yr. HD 75898c has $a_{\rm max} = 470$ AU and $P_{\rm max} = 7400$ yr. The possible stellar orbits for HD 5319c and HD 75898c are summarized in Table 5. Note that these orbit determinations are extremely uncertain, as we are using a 3 yr observational baseline to characterize orbits in the 10^2–10^4 yr range.

5. DISCUSSION AND CONCLUSIONS

We have discovered two Jovian-mass planets in Earthlike orbits, 1 AU $< a <$ 2 AU, orbiting the stars HD 5319 and HD 75898. Target selection of both stars was performed by the N2K Consortium (Fischer et al. 2005). For HD 75898, which was observed as part of the N2K low-resolution spectroscopic survey (Robinson et al. 2007), we find good agreement between the N2K and Keck atmospheric parameter estimates.

At 1.56 $M_\odot$, HD 5319 is on the verge of being a "retired" A-star ($M_\star > 1.6\ M_\odot$) of the type discussed by Johnson et al. (2007). In all nine previously known former A dwarf planetary systems, the planets orbit at semimajor axes $a \geq 0.78$ AU. HD 5319b fits this pattern well, with $a = 1.75$ AU. Although the total number of known planet hosts with $M > 1.6\ M_\odot$ is small, Johnson et al. concluded that the dearth of short-period planets around these stars is real, and the semimajor axis distributions of planets orbiting intermediate-mass and low-mass stars are different. Furthermore, engulfment by the expanding subgiant can only explain the disappearance of planets orbiting at $a < 30\ R_\odot$. Burkert & Ida (2007) point out that the lack of short-period planets orbiting intermediate-mass stars can be explained if these stars' protostellar disks have a shorter depletion timescale than their low-mass counterparts.

Among orbits larger than the tidal circularization cutoff of 0.1 AU, circular orbits, while not rare, are certainly not preferred. Butler et al. (2006) report that the distribution of eccentricities is nearly uniform beyond 0.3 AU. However, Meschiari et al. (2007) performed a blind experiment where they presented users of the Systemic[10] RV-fitting console with synthetic RV data sets drawn from circular orbits. The recovered eccentricity distributions had median values between 0.1 and 0.2, indicating a bias toward finding eccentric orbits. If the median exoplanet eccentricity has been skewed higher than its true value by the planet discovery process, solar system—like orbits, which seem noteworthy in the context of so many eccentric exoplanets, may be quite common. With 1 AU $< a <$ 2 AU and $e \approx 0.1$, HD 5319b and HD 75898b have orbits quite similar to our own terrestrial planets.

HD 5319 and HD 75898 have RV residuals that imply additional companions in the system. To account for our measured center-of-mass accelerations, HD 5319c and HD 75898c must both be at least 1 $M_{\rm Jup}$. If the periods and masses of these objects are near the minimum values recorded in Table 5, further RV observations might add these stars to the known list of multiple-planet systems within a few years. However, it is likely that these objects have periods too long for RV follow-up. In that case, HD 5319 and HD 75898 are good candidates for high-resolution imaging. The NIRC-2 coronagraph spot size is 0.5″, which would restrict the detection space to $a > 50$ AU for HD 5319 and $a > 40$ AU for HD 75898. With the NIRC-2+AO limiting contrast ratio of 0.1%, this detection space includes massive brown dwarfs and low-mass stars. The analytical work of Matzner & Levin (2005) supports the hypothesis that protostellar disk fragmentation is not a viable formation mechanism for star—brown dwarf binary pairs. HD 5319 and HD 75898 could therefore serve as laboratories for investigating the presumably rare phenomenon of brown dwarf formation in protostellar disks.

S. E. R. thanks Eugenio Rivera and Peter Bodenheimer for helpful input on this work. We gratefully acknowledge the dedication and support of the Keck Observatory staff, in particular Grant Hill for support with HIRES. We thank the NASA and UC Telescope assignment committees for generous allocations of telescope time. The authors extend thanks to those of Hawaiian ancestry on whose sacred mountain of Mauna Kea we are privileged to be guests. Without their kind hospitality, the Keck observations presented here would not have been possible. The authors have made use of the SIMBAD database, the Vienna Atomic Line Database, and NASA's Astrophysics Data System.

This research is made possible by the generous support of Sun Microsystems, NASA, and the NSF. S. E. R. was supported by the National Science Foundation Graduate Research Fellowship. G. L. received support from the NSF Career grant (0449986). S. S. V.'s work was supported by the NSF grant AST 03-07493. D. A. F. was supported by Research Corporation's Cottrell Science Scholar program and by NASA grant NNG 05-G164G. We thank the Michelson Science Center for travel support through the KDPA program.

Facilities: Keck:I (HIRES)

[10] See http://oklo.org.

REFERENCES

Ammons, S. M., Robinson, S. E., Strader, J., Laughlin, G., Fischer, D., & Wolf, A. 2006, ApJ, 638, 1004

Bevington, P. R., & Robinson, D. 1992, Data Reduction and Error Analysis for the Physical Sciences (2nd ed.; New York: McGraw-Hill)

Boss, A. P., et al. 2007, Trans. IAU, 26, 183

Burkert, A., & Ida, S. 2007, ApJ, 660, 845

Butler, R. P., Marcy, G. W., Williams, E., McCarthy, C., Dosanjh, P., & Vogt, S. S. 1996, PASP, 108, 500

Butler, R. P., et al. 2006, ApJ, 646, 505

Cumming, A. 2004, MNRAS, 354, 1165

David, E.-M., Quintana, E. V., Fatuzzo, M., & Adams, F. C. 2003, PASP, 115, 825

Eaton, J. A., Henry, G. W., & Fekel, F. C. 2003, in The Future of Small Telescopes in the New Millennium, Volume II—The Telescopes We Use, ed. T. D. Oswalt (Dordrecht: Kluwer), 189

Eggenberger, A., & Udry, S. 2007, in Planets in Binary Star Systems, ed. N. Haghighipour (Berlin: Springer), in press (arXiv:0705.3173)

Endl, M., Cochran, W. D., & Wittenmyer, R. A. 2006, AJ, 131, 3131

ESA. 1997, The *Hipparcos* and Tycho Catalogs (ESA-SP 1200; Noordwijk: ESA)

Fischer, D. A. et al. 2005, ApJ, 620, 481

———. 2006, ApJ, 637, 1094

———. 2007, ApJ, 669, 1336

Grether, D., & Lineweaver, C. H. 2006, ApJ, 640, 1051

Henry, G. W. 1999, PASP, 111, 845

Johnson, J. A., et al. 2006, ApJ, 647, 600

———. 2007, ApJ, 665, 785

Kjeldsen, H., & Bedding, T. R. 1995, A&A, 293, 87

Matzner, C. D., & Levin, Y. 2005, ApJ, 628, 817

McCarthy, C., & Zuckerman, B. 2004, AJ, 127, 2871

Meschiari, S., et al. 2007, ApJ, submitted

Noyes, R. W., Hartmann, L., Baliunas, S. L., Duncan, D. K., & Vaughan, A. H. 1984, ApJ, 279, 763

Patel, S. G., Vogt, S. S., Marcy, G. W., Johnson, J. A., Fischer, D. A., Wright, J. T., & Butler, R. P. 2007, ApJ, 665, 744

Pourbaix, D., et al. 2004, A&A, 424, 727

Robinson, S. E., Ammons, S. M., Kretke, K. A., Strader, J., Wertheimer, J. G., Fischer, D. A., & Laughlin, G. 2007, ApJS, 169, 430

Sato, B., et al. 2005, ApJ, 633, 465

Takeda, G., Ford, E. B., Sills, A., Rasio, F. A., Fischer, D. A., & Valenti, J. A. 2007, ApJS, 168, 297

Valenti, J. A., & Fischer, D. A. 2005, ApJS, 159, 141

VandenBerg, D. A., & Clem, J. L. 2003, AJ, 126, 778

Vogt, S. S., et al. 1994, Proc. SPIE, 2198, 362

Wright, J. T. 2005, PASP, 117, 657

Wright, J. T., et al. 2007, ApJ, 657, 533

Yi, S., Demarque, P., Kim, Y.-C., Lee, Y.-W., Ree, C. H., Lejeune, T., & Barnes, S. 2001, ApJS, 136, 417